Master's Thesis

MICROFLUIDIC BIOREACTOR ARRAY FOR ADVANCED MICROBIOLOGICAL HIGH THROUGHPUT SCREENING WITH THROUGH HOLE MEMBRANE

Janghyun Ju

Department of Biomedical Engineering

Graduate School of UNIST

2020

MICROFLUIDIC BIOREACTOR ARRAY FOR ADVANCED MICROBIOLOGICAL HIGH THROUGHPUT SCREENING WITH THROUGH HOLE MEMBRANE

Janghyun Ju

Department of Biomedical Engineering

Graduate School of UNIST

MICROFLUIDIC BIOREACTOR ARRAY FOR ADVANCED MICROBIOLOGICAL HIGH THROUGHPUT SCREENING WITH THROUGH HOLE MEMBRANE

A thesis
submitted to the Graduate School of UNIST
in partial fulfillment of the
requirements for the degree of
Master of Science

Janghyun Ju

December. 13. 2019
Approved by

Advisor
Taesung Kim

MICROFLUIDIC BIOREACTOR ARRAY FOR ADVANCED MICROBIOLOGICAL HIGH THROUGHPUT SCREENING WITH THROUGH HOLE MEMBRANE

Janghyun Ju

This certifies that the thesis/dissertation of Janghyun Ju is approved.

December. 13. 2019

Advisor: Taesung Kim

Sung Kuk Lee

Tae Eun Park

Abstract

Recently, biological analysis has been revolutionized with micro-/nanofluidic system in precise measurement and repeatable testing. Especially, microbial engineering in a high-throughput manner provides a novel means to single cell level analysis, cytotoxicity test or metabolic system studies. Microwell array that one of representative microfluidic platform was widely used and commercialized to screening cell-free reagents or rare cells with mutant libraries. It is convenient to microbial handling such as cell immobilization, optics-based observability, and target cell isolation. However, the throughput is limited to the size of the unit microwell and the spacing distance between neighboring microwells.

In this study, I developed a novel microwell array that is covered with a thin brittle layer on one side and has an individual open access hole to supply additional nutrients or inducers with trapped cells on the other side. It was fabricated by integrating a heterogeneously surface processed and stepped through-hole membrane into a microfluidic device. The outer surfaces were treated to be hydrophobic and inner ones to be hydrophilic, resulting in the robust and cross-contamination-free partitioning of cell suspension.

There were multi-functions for high-throughput microbial handlings, and it can be realized via stepped through-hole (ST) and double-sided (DS) microwells. ST structure acts as a narrow outgoing entrance and prevents sample leakage by obstructing the interference of external fluid flow in buffer exchange. Furthermore, Hydrophobic-In-Hydrophilic (HIH) induces the selective condensation by topological liquid pinning and low wettability for chemical dosing. Meanwhile, DS microwells selectively open by locally breaking their cover layer with a microneedle, and then target microbes are successfully extracted out through the punched vertical microchannels. The cell extractor was customized for non-cell hazardous, but high-precision with less than 1 μm resolution. For practical demonstration of high-throughput screening (HTS), I proceeded the proof of concept experiment with rare cell isolation test using two components cell mixture of which the population ratio was about 1 to 10^6.

The proposed multifunctional high-throughput bioreactor has been optimized for automated screening system. The throughput was increased to 1.5×10^5 microwells in 3.8 cm × 5.5 cm area, cell-friendly target extraction was developed for broaden applicable cells, and high-throughput screening operation time such as partitioning, multi-well dosing, target scanning was minimized. Thus, I ensure that it can be used as a practical tool for mutant library analysis including CRISPER, quality by design (QbD), next-generation sequencing (NGS), and target cell sorting.

Table of Contents

List of Figures

Figure 8. Working principle of Double-Sided microwell array. The schematic shows microbial handling procedure for high-throughput screening at cross-sectional side view of the device. (a) Loading the microbial cell suspension after PDMS substrate in a vacuum condition. (b) Dewetting by the hydrophobic surface causes instantaneous partitioning between microwells. (c) Incubated microbial cells in high humidity to prevent dehydration. (d) By forming crack-based vertical channel via a microneedle, microbes with target mutant libraries were grown and spontaneous extracted through H-PDMS hole.

Figure 9. Partitioned FITC solution in different humidity conditions. The fluorescence images show partitioned FITC solution in different humidity conditions. There was no noticeable evaporation of liquid at high humidity (RH = 95%) over 24 hours, in contrast to the low humidity (RH = 60%).

Figure 10. Scraping handling with hydrophilic devices. The plasticized Ostemer can withstand the pressing force to preserve the sample when scraping handling. However, as the distance between microwells was decreased, neighboring microwells was connected by liquid bridges and it may cause the cross-contamination. (Scale bar : 100 μm)

Figure 11. HIH surface modification process and characterization. (a) Each different resultant surface with the fluoropolymer, Ostemer, and H-PDMS is highlighted in magenta, cyan, and blue. Wettability of the three different surfaces was measured to 99.4 ± 3.2°, 21.6 ± 1.1°, and 50.4 ± 0.7°, respectively. (b) Time-lapse image of surface modification with/without stepped through-hole structure shows the inner penetration of fluoropolymer and selectively surface modified. (w/ hole interval time : 0.5 sec, w/o hole interval time : 2.5 sec)

Figure 12. SAM image of HIH surface modified microwell cross-sectional side view. the microwell interior was treated with oxygen plasma and attached the amine group on the treated surface using aqueous 10% APTES and small hole side surface was deposited with 3M Novec 1720 fluoropolymer. The functionalization of APTES was determined by attachment of 200-nm carboxylated polystyrene nanoparticles. (Scale bar : 10 μm)

Figure 13. Self-partitioning with GFP microbial cells in LB. Red dash line represented liquid-air phase and self-partitioning occurred in 0.5 seconds.

Figure 14. Recent target cell extraction methods using optical instruments. (a) The specific region of photo-degradable hydrogel (PEG hydrogel) was dissolved by UV [35]. (b) The cured agarose droplet in microwells was detached with the strong heat generation by infrared laser and extracted with an additional medium flow [36].

Figure 15. Automatic cell extractor for target isolation in high-throughput screening. (a) Real image of customized cell extractor. The bottom shows the punched H-PDMS layer and crack-based vertical channel forming process. (b) It describes the order of automated extraction process controlled by LabVIEW-based software. (c) Demonstration of cell extractor for high-precision using FITC solution. (PBS 1X, 0.01% F-127)

Figure 16. Partitioned FITC solution with LB cover. 3 hours later, the absence of LB cover shows dark gray circle that evaporated site compared with presence of LB cover.

Figure 17. Hatching-like isolation process with voluntary extracted cells. The image of spontaneous escaped bacteria in the vertical microchannels was taken in 2730 sec at 30X magnification.

Figure 18. Characterization of hatching-like isolation. (a) The FITC solution (PBS 1X, 0.01% F-127) mass transfer rate with diffusion was described with the fluorescence intensity graph. Sky blue box indicates handling time period after punching process. (b, c) GFP and RFP fluorescence images of different focal points for selective extraction confirmation. Each of them indicates before extraction state and the result of forming vertical microchannels with incubated 6 hours.

Figure 19. Schematic chemical dosing and time-lapse image of vapor supply by condensation. Red arrows in the bright-field image highlight the diameter of the liquid-air interface formed in the microwell, showing a decrease in the diameter during condensation.

Figure 20. Schematic illustrations and fluorescence images of buffer exchange. The device was immersed in clean water and washed out FITC (PBS 1X, 0.01% F-127) from the microwells. Red arrows in time-lapse images highlight the RFP cells to show the constant number even after repartitioning.

Figure 21. High-throughput screening demonstration with rare cell isolation. (a) The cell composition ratio of extracted samples with hatching-like isolation method. There were two screening cycles in total, and the GFP cell composition ratio increasing from 0.00013% to 0.73% and 100%, respectively. (b) fluorescence image in each screening culture. The 1st screening was diluted with an average of 90 cells per chamber to increase throughput, whereas 2nd screening was performed with dilution to single cell level to increase the precision of cell selectivity.

Figure 22. 1st screening large area scanning result and cell composition image. (a) The image was taken at 10X magnification, and each photographic piece were combined with image stitching technique. Consequently, 12 coordinates of target microwell were detected in 1st screening scan data. (b) Fluorescence image of cell composition in each screening cycle with 10 μm height microchannels.

List of Tables

Nomenclature

Amp: ampicillin
APTES: (3-aminopropyl) triethoxysilane
Bio-MEMs: micro electro mechanical system for bio application
CCD: charge coupled device
CRISPER: clustered regularly interspaced short palindromic repeats
RNA: ribonucleic acid
DS: double-sided
D.W: distilled water
E. coli: *Escherichia coil*
FACs: fluorescence activated cell sorting
FITC: fluorescein isothiocyanate
GFP: green fluorescent protein
GPTMS: (3-Glycidyloxypropyl)trimethoxysilane
HIH: hydrophobic-in-hydrophilic
HMIs: heavy metal ions
H-PDMS: Hard-PDMS
HTS: high-throughput screening
LB: Luria-Bertani broth
LT point: left top point
Ostemer: off-stoichiometry thiol-ene polymer
PBS: phosphate buffered silane
PCR: polymerase chain reaction
PDMS: polydimethylsiloxane
PEG: poly ethylene glycol
pH: potential of hydrogen
PS NPs: polystyrene Nanoparticles
QS: quorum sensing
RB point: right bottom point
RFP: red fluorescent protein
RH: relative humidity
SEM: scanning electron microscope
ST: stepped through-hole
UV: ultraviolet

I. Introduction

1.1 Microfluidic Approaches for Biological Research

Microfluidic creates a dynamic cell culture environment by manipulating the fluid system. Various biological studies that quorum sensing, metabolic engineering, genomics, cytotoxicity test was proceeded with bio-MEMs and it is now a fundamental necessity in microscopic bio-analysis [1-3]. First, miniaturization can be carried out experiments in small laboratory scale and cost-effective with low reagent consumption. Unlike the earlier biological experiments that were tested with large flasks, consumption with a micro/nano-scale volume was useful to design experiments if the reagents are expensive or difficult to obtain [4-7]. In addition, high density-to-volume provides the rapid chemical reaction or cellular response [8-9]. Second, microfluidic was highly effective for quantitative analysis with high-precision. For example, Minseok Kim et al. developed a chemostat-like microbial biosensor for HMIs (Heavy Metal Ions) detection [10]. Genetic-modified *E. coli* cells were trapped with arrowhead-shaped ratchet structures and measured the detection sensitivity with concentration gradient. They compiled data on fluorescence signal strength by HMIs concentration, and then suggested the correlation between fluorescent intensity and concentration of Cd^{2+}. Third, automation and parallelism reduce the number of repeatable test and increase the efficiency. This is botherless from manual labors and shows scale up feasibility by running thousands of identical experiment with a single chip. Liu et al. developed a microfluidic device that automatically parallel loading the multiple reagents with capillary force [11].

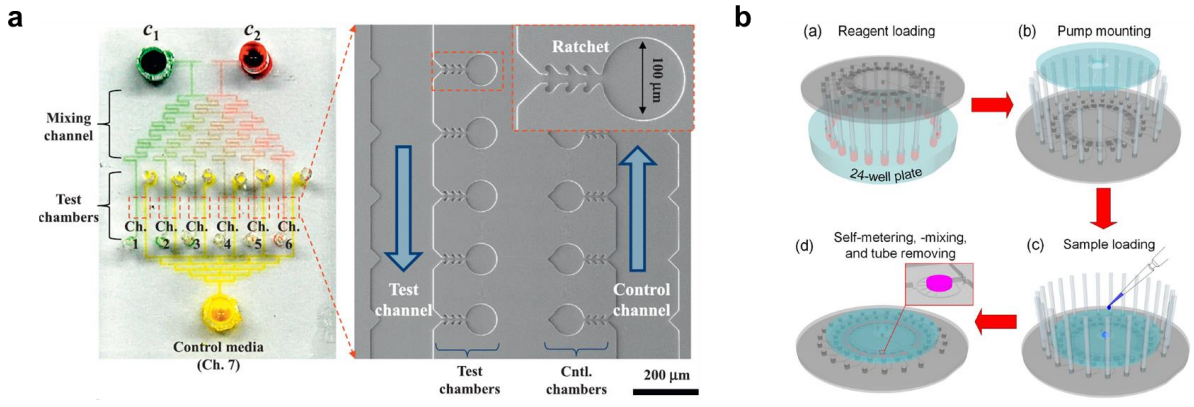

Figure. 1 Quantitative and parallel technologies with microfluidics. (a) The microchannels with Christmas tree structure was used to generate quantitative concentration gradient and investigate the microbial sensitivity of heavy metal ion detections [10]. (b) 24 different reagents were sucked into glass microtubes by capillary force and negative-driven pressure of PnP (place and play) pump PDMS leads that loading sample and reagents were aspirate to microchannels [11].

1.2 High-throughput studies with Microfluidics

High-throughput is a widely used experimental technique that lots of chemical, genetical, and pharmacological samples were analyzed in parallel. Numerous throughput study has been conducted, ranging from 96 microplates in 1980 to tens of million throughputs with droplet microfluidics. The analysis time, which would take several days, was reduced to just a few hours with a high-throughput microfluidic device, and various studies such as flow cytometry, droplet microfluidics, microwell array were developed to increase the throughput.

Fluorescence-activated cell sorting (FACs) detects the different cell size, composition, and specific functionality, and then sorts the target samples [12-13]. The cell suspension was processed in laminar state and protected from external physical stress while the sample is being transported. It screened with the rate of 30,000 cells/second and boasted high screening purity. However, this method was confined to fluorescent-labeled detection and has a risk of contamination due to off-chip process.

Droplet microfluidics is a recently developed versatile technology that generated several million droplets spontaneously with immiscible oil-water phase system. In point of care bio-medical fields, droplet microfluidic was now prominent in that ultra-high-throughput for rapid detection of infectious bacteria in bloods [14-15]. Although droplet microfluidics are useful to automation and high-throughput, there were some fundamental limitations. Basically, droplet microfluidic platform design, which includes mixing, pumping, focusing and sorting, was very complex and requires expert handlings. Thus, it is hard to realize the commercialization and additional functions such as cell lysis or PCR for subsequent investigation can be burden [16].

Microwell array is the most popular and representative high-throughput microfluidic platform. One of reasons that is preferred was stable to cell immobilization in specific area. Spatial constraints of the cell movement provide convenient especially in non-adherent cells [17]. Also, fusion with other optical, electrical, physical equipment enables advanced investigation. G. Lemercier et al. has opto-electrochemical analysis of mitochondrial function by measuring the amount of dissolved oxygen and hydroperoxide in the wells through the nanoelectrodes [18]. Lastly, spatiotemporal single cell analysis of single cell dynamics is possible because the behavior and movement of both mother and daughter cells are observed in real time with microscopy [19]. As the importance of single cell study has been emerged, the microwell array was conspicuous in that target cell behavior pattern, differentiation rate, generational variation, nutritional consumption, and by-product characteristics can be performed. However, state of the art microwell array still has bottleneck that throughput is limited by 10^3~10^4 microwells in the 30 cm^2 region.

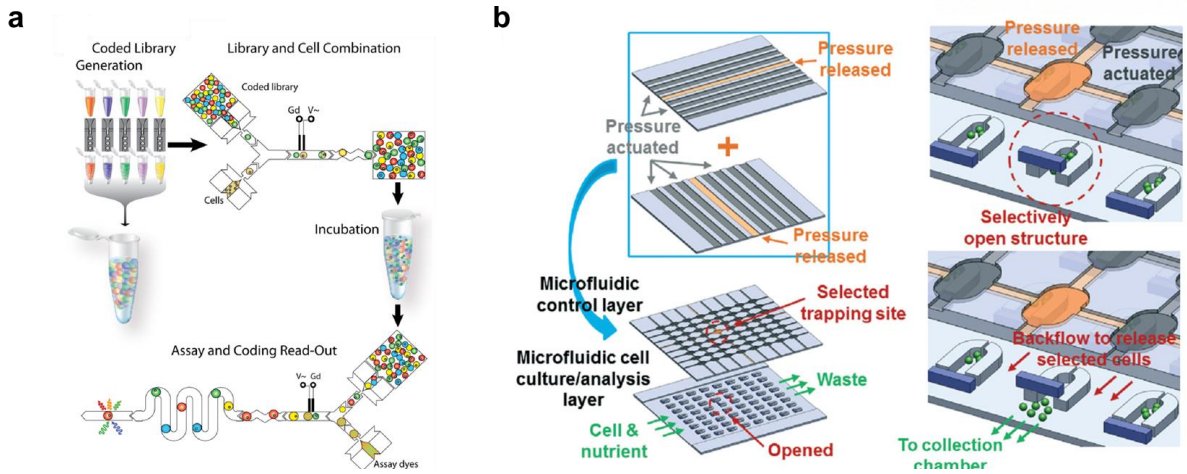

Figure 2. Microfluidic high-throughput technologies. (a) Ultra-high-throughput droplet microfluidics for cytotoxic screening that can produces 100 droplets per second [20]. It shows multiplex assay by emersion mammalian cell droplet with different concentration of Mitomycine C. (b) High-throughput microwell array platform for single-cell screening that can extracted target cells with actuated microchannels by hydraulic pressure and possible to further analysis [21]. The throughput was increased by multi-layer stacking and 32×32 (=1024) trapping sites were fabricated.

1.3 Microbial Handling in High-throughput manners

Microorganism in nature is so immense that there were over 10^9 living species [22-23]. In microbial engineering, identification of each single entity has been important in high-throughput manners to describe cellular functionalities [24-25] or discriminate genetically synthesized cells having industrially valuable bio-refineries [26]. To tackle the demand, microfluidic effort to replace labor-intensive conventional microbial studies [27-28], but several technical challenges remained and coupled with the reliability of engineering microbes. First, occasionally lots of liquid bridge between neighbor microwells occurred in the most common partitioning method such as liquid scraping [27, 29-30]. Recently, selective surface modification for fabricating hydrophilic-in-hydrophobic microwell enables to spontaneously generate discretized liquid without the bridged defects [31-32]. Unfortunately, it is difficult to chemically functionalize hydrophilic surfaces for customization keeping hydrophobic parts intact, or these require costly multi-lithographic processes. Second, multiple chemical dosing without cross contaminations has been relied on microscale planar alignment of external microstructures, which becomes error-prone, cumbersome and costly in proportional to density of bioreactors [33]. Third, extraction at microscale have been lacked automation and isolation of intact cell. Capillary extraction process requires skillful handling and suffer from fast evaporation during transport of nanoliter aqueous samples [27, 35]. On the contrary optical extraction methods enabled the simple automation, but the lights may result hazardous to cells [35-36]. By all accounts, in order to increase the throughput of microwells, simple and effective partitioning or high-resolution but low cytotoxic cell extraction was required.

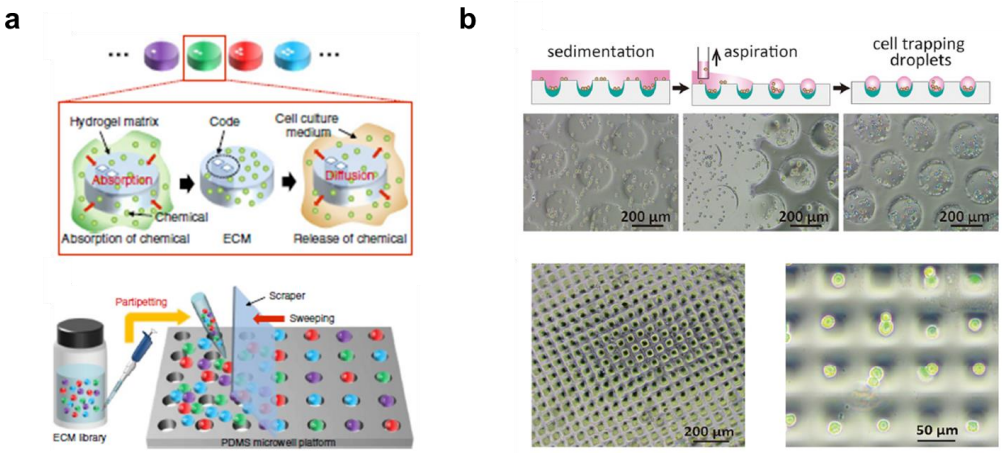

Figure 3. Scraping Handling and aspiration with selective surface modified device. (a) Scraping handling is widely used common partitioning method that separated each microwells to prevent cross-contamination [30]. Depending on the user's strength, the PDMS microwells are at risk of crushing. (b) Hydrophobic-in-hydrophilic surface encourages self-partitioning in aspiration process. Hydrophobic surface breaks the liquid bridges between microwells [31].

II. Fabrication and Characterization of Double-Sided Microwell Array

2.1 Experimental Methods

2.1.1 Reagents and materials

PDMS (Sylgard 184, Dow Corning), Ostemer resin (Ostemer 322 Crystal Clear, Mercene Labs), and H-PDMS, including 3.4 g vinylmethylsiloxane-dimethylsiloxane trimethylsiloxy-terminated copolymer (VDT-731, Gelest), 18 μL platinum catalyst (JSI silicone), and 20 μL 2,4,6,8-tetramethyltetravinylcyclotetrasiloxane (Sigma-Aldrich), were used to fabricate the microwell array. Trimethylchlorosilane (92361, Sigma-Aldrich), trichloro(1H,1H,2H,2H-perfluorooctyl)silane (PFTS; 448931, Sigma-Aldrich), (3-Aminopropyl)triethoxysilane (APTES; 440140, Sigma-Aldrich), (3-Glycidyloxypropyl)trimethoxysilane (GPTMS; 440167, Sigma-Aldrich), and fluoropolymer (Novec F-1720, 3M) were used for surface modifications of the microwell array. To prepare solutions for characterizing the microwell array, 200-nm carboxylated PS NPs (Polysciences), FITC (F7250, Sigma-Aldrich), pluronic F-127 (P2443, Sigma-Aldrich), and phosphate-buffered saline (PBS; P5493, Sigma-Aldrich) was used. In bacterial culture, LB-Miller, Tryptone Broth (TB), and agar were purchased from BD Biosciences. All the percentage scales for solutions are in the weight/volume percentage in this work.

2.1.3 Preparation of bacteria cells

Two Escherichia coli MG1655 strains were harboring plasmids pTKU4-2 and pTKU4-65 expressing GFP and RFP, respectively. the GFP and RFP cells were used to characterize the microwell array. For cell culture, it was followed the standard bacterial culture process. A single colony grown on an LB agar plate was picked, and a culture tube was filled with 5 mL of LB medium. All cultured cells were incubated for about 18 hours in a shaking incubator (180 rpm, 37 °C). Cell densities were quantified by counting the numbers of all GFP and RFP cells in a known volume of 10-μm height microchannels.[37] GFP and RFP cells in the stationary phase were used to demonstrate their partitioning in the microwells.

2.1.3 Fabrication of the double-sided microwell array

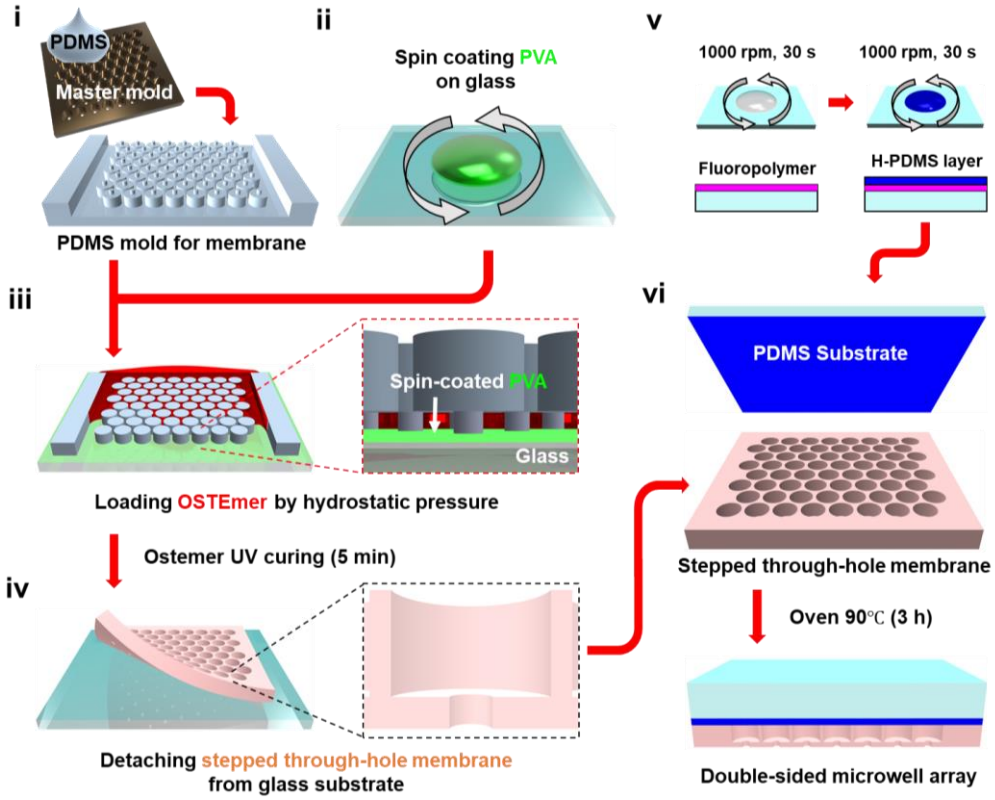

Figure 4. Fabrication processes of the ST membrane and DS microwell array.

The working flow to fabricate the device is summarized in Figure 4. the SU-8 master was prepared with two-layered patterns of SU-8 photoresist (SU-8 2025 and SU-8 2050, MicroChem), using the common processes of photolithography. The PDMS (Sylgard 184, Dow Corning) mold was made with following common soft-lithography processes, followed by functionalization of its surface with chlorodimethylsilane (*Figure 4.i*). After preparing the glass coated with polyvinyl alcohol (PVA) using a spin coater for making a water-soluble sacrificial layer (*Figure 4.ii*), the PDMS mold was placed on the PVA-coated glass (*Figure 4.iii*). Inclining the PDMS mold on the glass to generate hydrostatic pressure, the Ostemer resin was loaded in the microfluidic channel. Because of van der Waals interaction, the PDMS mold and PVA layer remained in contact conformally during Ostemer resin loading. After solidifying the Ostemer resin with ultra-violet (UV, 312 nm) light for 5 min, the PDMS mold was removed (*Figure 4.iv*). The PDMS mold was reusable. To detach the UV-cured membrane from the glass substrate, the PVA sacrificial layer was dissolved in water. In parallel, the fluoropolymer was spin-coated on PDMS at 1000 rpm for 30 s, and sequentially, h-PDMS was coated with a spin coater at 1000 rpm for 30 s (*Figure 4.v*). Then, the surface of H-PDMS was functionalized with GPTMS. Finally, the membrane was chemically bonded with H-PDMS, after baking of the membrane at 90 °C in an oven (*Figure 4.vi*).

2.1.4 Experimental setup

An automated three-axis manipulator for the hatching-like extraction process comprised a motorized Z-stage (8MTF, Standa), motorized XY-stage (8MVT100-25-1, Standa), and a dovetail stage (MC1D-60, GMT). Each motorized XY stage and Z stage had a resolution of 0.31 μm, 0.625 μm, respectively. In the manipulator setup, the insulin needle (BD Biosciences) can be placed and controlled with the Z-stage, and the position of microwells can be controlled with the stage. A USB microscope (AM7915MZTL, Dino-lite) is embedded in the automated manipulator to monitor the place of the microwell array. The software for automation has been customized to operate our system, based on the Labview (National Instruments) software development kit (SDK) files of the USB microscope from Dino-lite and the motorized stage from Standa.

Our optical and fluorescent images were captured using a CCD camera (Clara Interline CCD, Andor Technology Ltd) mounted on an inverted fluorescence microscope (IX71, Olympus Corp.). The microscope was automated using a motorized stage (BioPrecision2), a motorized focus controller (99A400), and a controller system (MAC 5000), which were manufactured by Ludl Electronic Products. SEM images were obtained using a field-effect scanning electron microscope (FE-SEM; S-4800, Hitachi). To control the atmospheric conditions, a customized humidity/temperature controlling system, comprising solenoid valves (S10MM-20-24-2, Pneumadyne Inc.), a humidity/temperature sensor (SHT15, SENSIRION), a microcontroller board (Arduino Uno, Arduino cc.), and a microscope incubator (CU-501, Live Cell Instrument), was programmed using LabVIEW software (National Instruments).

2.2 Double-Sided Microwell Array Structure

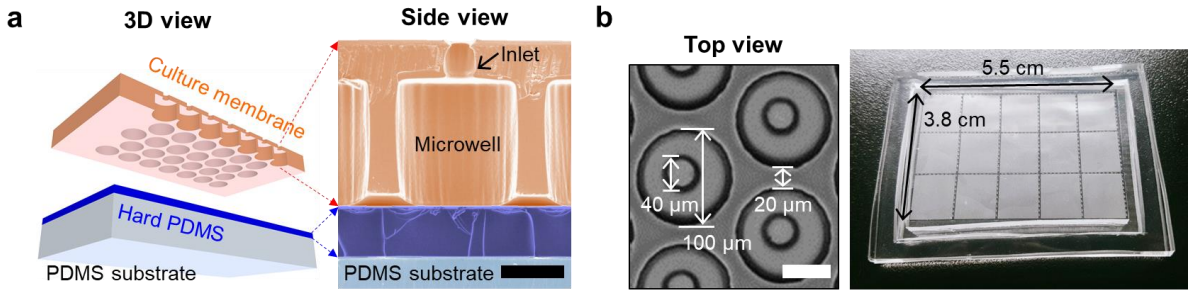

Figure 5. Schematic of Double-Sided microwell array structure. (a) 3D illustration of the device and SAM image of side view. (Scale bar : 50 μm) (b) Microscope image of top view and real dimension of the bioreactor. (Scale bar : 60 μm)

Microwell array was consisted of culture membrane and Hard-PDMS(H-PDMS), in which 150,000 microrwells were fabricated in an area of 3.8 cm × 5.5 cm. Each membrane and H-PDMS layer

thickness was 140 μm and 50 μm. The monolithic stepped through-hole (ST) membrane is made with a robust off-stoichiometry thiol-ene polymer (Ostemer), and its design is equivalent to the layering of two through-hole membranes (*Figure 5.a*). The size of each hole is respectively 40 μm and 100 μm in diameter and 30 μm and 100 μm in height (*Figure 5.b*). H-PDMS, which described with dark blue, wrapped the large hole side of ST membrane and has a fragile physical property, so that it can be easily selective-opened with punch-hole extraction method. On the other hand, the small holes are ordinally open type inlets that enable sample loading, surface modification, and chemical dosing.

	Curing Method	Young's Modulus	Surface Property
OSTEmer	1st Curing : UV Photo-Curing 2nd Curing : Thermal-Curing	1000 MPa	After 1st Curing : SH- and Epoxy groups After 2nd Curing : OH- groups
PDMS	Only Thermal-Curing	360-870 KPa	After O_2Plasma : OH- groups

Table 1. Characteristics of used material. This table based on product data sheet and reference paper.[38] Both materials were bio-compatible, but surface properties and young's modulus were different. Ostemer has plasticized properties and high young's modulus, so that its high structural stability prevents the sample leakage during extraction process.

The reasons of selecting Ostemer materials for fabricated the bioreactor are shown in the following Table 1. PDMS material has one-step curing process and easy to be manufacture, but the high strain suggests unstable deformation. Whereas Ostemer owned high young's modulus of approximately 2000 times of PDMS, so that it has high structural stability. The punch hole based physical extraction method, which developed in this study, can occur structural deformation and sample leakage when the microwells were punched with a microneedle. Fabrication with plasticized Ostemer material is better suitable during extraction process and easy to be handling.

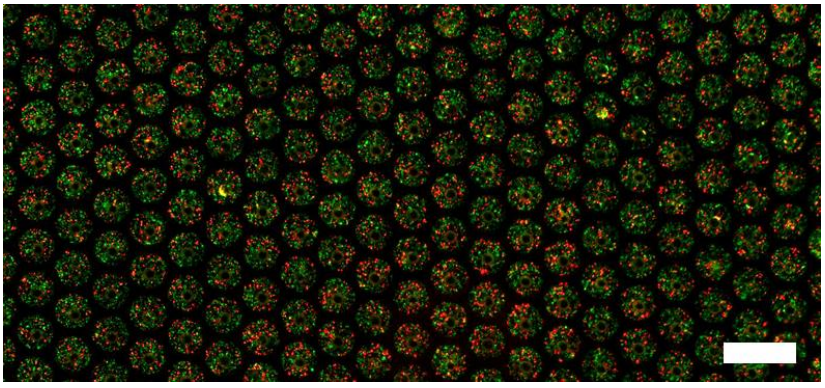

Figure 6. Co-culture Fluorescence image with Double-Sided microwell array. (Scale bar : 100 μm)

The distance between neighboring microwells was compacted to 20 μm and partitioning was perfect with HIH surface treatment. It will be described later in detail. For amicable growth environment, 0.8 nL high-contents volume of microbial sample can be loaded and cultured in the device. For example, two genetic modified microbial cells were co-cultured in microfluidic chips as shown in figure 6.

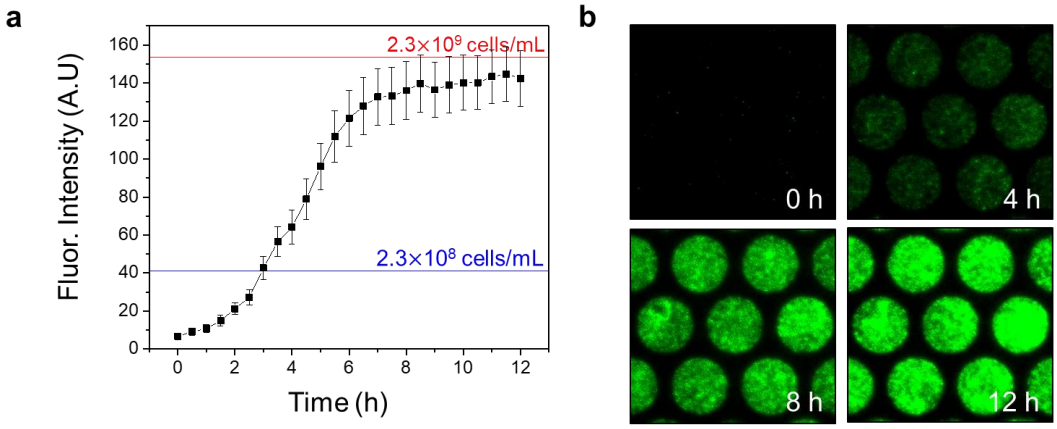

Figure 7. Microbial cell culture characterization. (a) fluorescent intensity graph of GFP cell culture in double-sided microwell array. Red line indicated cell density of stationary phase sample in shaking incubator and blue line was $\frac{1}{10}$ diluted sample of them. (b) GFP fluorescence images of GFP cell culture at 4 hours intervals.

18 hours cultured GFP cells, which grown in shaking incubator, has 2.3×10^9 cells/mL cell density. The growth environment of the microfluidic device was characterized as compared to the cell density of the control group. The culture time in microfluidic device was 13 hours, and stationary phase of the microbial growth curve was observed to form at 9 hours (*Figure 7.a*). The growth rate was measured by relative fluorescence intensity, and each of GFP and RFP cells were confirmed 2.2×10^9 cells/mL and 1.8×10^9 cells/mL, respectively (*Figure 7.b*).

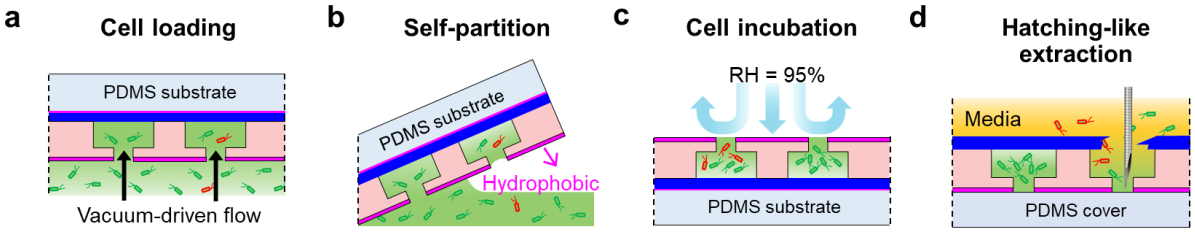

Figure 8. Working principle of Double-Sided microwell array. The schematic shows microbial handling procedure for high-throughput screening at cross-sectional side view of the device. (a) Loading the microbial cell suspension after PDMS substrate in a vacuum condition. (b) Dewetting by the hydrophobic surface causes instantaneous partitioning between microwells. (c) Incubated microbial cells in high humidity to prevent dehydration. (d) By forming crack-based vertical channel via a microneedle, microbes with target mutant libraries were grown and spontaneous extracted through H-PDMS hole.

There were four steps of microbial handling for high-throughput screening. Sample loading of batch type microwell array was performed using a negative pressure of vacuum (*Figure 8.a*). Since PDMS is a porous material, the vacuum space of PDMS generates suction power. Using the vacuum-driven force (13 Pa, 15 min), microfluidic device floated on cell suspension fills microbial sample into microwells by themselves [39]. Self-partitioning was realized by hydrophobic-in-hydrophilic (HIH) surface modification (*Figure 8.b*). Fluoropolymer was selectively coated on small hole side of surface because of topological liquid pinning induced by ST structure [40]. The hydrophilic interior is suitable to cell loading due to easy inflow of water, and hydrophobic outer surface as delineated with pink line promote partitioning by breaking the liquid bridges. As a result, this hydrophobic side can prevent cross-contamination between neighboring microwells. The HIH surface allows for self-partitioning by simply lifting the microfluidic device, so that no additional steps are required for partitioning. In incubation process, the face with the small holes forward to the air for abundant oxygen supply (*Figure 8.c*).

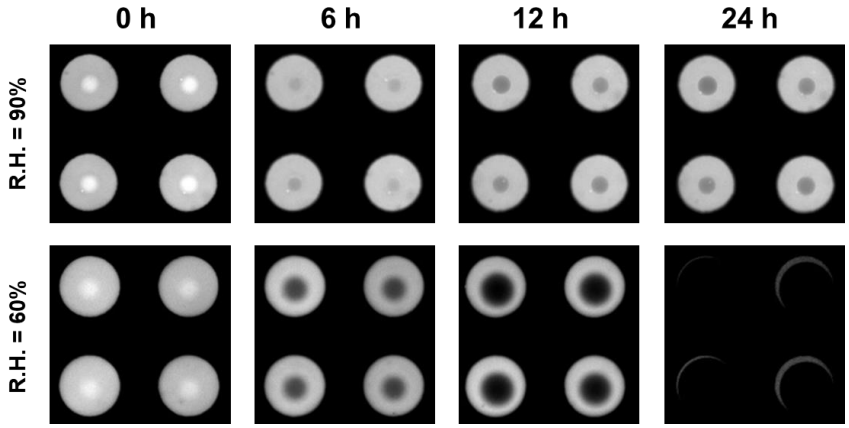

Figure 9. Partitioned FITC solution in different humidity conditions. The fluorescence images show partitioned FITC solution in different humidity conditions. There was no noticeable evaporation of liquid at high humidity (RH = 95%) over 24 hours, in contrast to the low humidity (RH = 60%).

However, the capacity of each microwell was about 1 nL, that was easy to evaporate, so that culture was performed inside the temperature and humidity controllable chamber (Temperature, T = 38°C, Relative humidity, RH = 95%), and it is also connected to the aeration valve to ensure a constant supply of fresh air (*Figure 9*). After screening, H-PDMS and culture membrane were disassembly from PDMS substrate and small hole side was laid on PDMS slab for extraction. H-PDMS was easily transferred from fluoropolymer coated PDMS substrate to culture membrane. Then, laid culture membrane was covered with fresh media that trapped with clean wall PDMS. Microwell with target microbes was automatically extracted using customized cell extractor (*Figure 8.d*). The cell extractor was manufactured for high-selectivity, high-precision and reduced processing time in high-throughput manners. It is punch hole based physical method and a 31 gauge diameter insulin syringe tip selectively

extracts 50 μm thick brittle H-PDMS on the target microwell. The bespoke software detects the cross align marker, which located in each corner of device, and find the coordinate of the target microwell by calibrating distance ratio between two diagonal cross markers. Cracks on the H-PDMS surface act as a vertical microchannel to connect the medium with the target microwell. A rich medium can be supplied through the holes made by the microneedle so that microbial cells be further breed and comes out from the microwell. The cells with target mutant library can be easily received by only pipetting those medium.

2.3 Hydrophilic-In-Hydrophobic Microwell Array Characterization

2.3.1 Hydrophilic-In-Hydrophobic Surface Modification

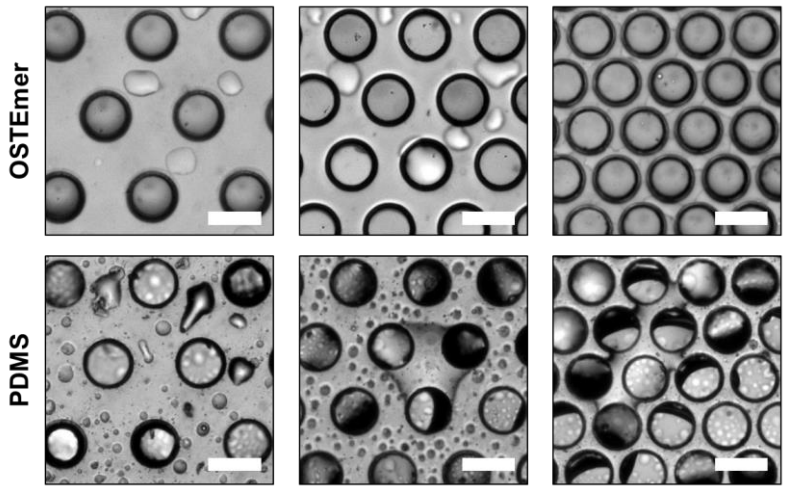

Figure 10. Scraping handling with hydrophilic devices. The plasticized Ostemer can withstand the pressing force to preserve the sample when scraping handling. However, as the distance between microwells was decreased, neighboring microwells was connected by liquid bridges and it may cause the cross-contamination. (Scale bar : 100 μm)

Generally, scraping handling is a widely used partitioning method in microwell array platform. Unfortunately, the higher the compactness of microwells, the higher the probability of forming liquid bridges between neighboring microwells (*Figure 10*). To tackle this problem, selective surface modification method for HIH was developed and discretized each microwells in an instant. However, the chemical surface functionality was limited in customization and it is possible even with high cost several steps of lithographic processes. Microchannel can be alternative, but sample may leakage to the microchannels during extraction process, resulting from poor physical accessibility.

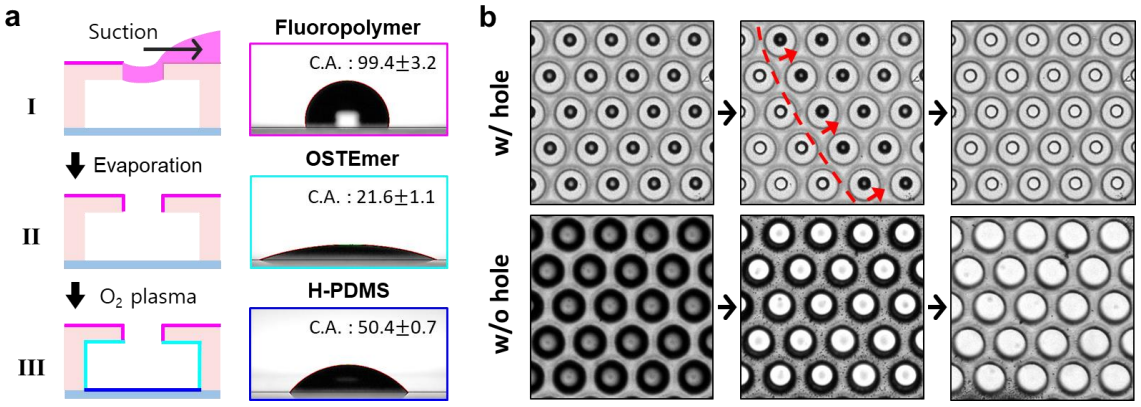

Figure 11. HIH surface modification process and characterization. (a) Each different resultant surface with the fluoropolymer, Ostemer, and H-PDMS is highlighted in magenta, cyan, and blue. Wettability of the three different surfaces was measured to 99.4 ± 3.2°, 21.6 ± 1.1°, and 50.4 ± 0.7°, respectively. (b) Time-lapse image of surface modification with/without stepped through-hole structure shows the inner penetration of fluoropolymer and selectively surface modified. (w/ hole interval time : 0.5 sec, w/o hole interval time : 2.5 sec)

HIH surface modification via ST structure was simple, low-cost, and solution-based processing. The volatile solvent containing the fluoropolymer 3M Novec 1720 was used and dropped on the side of small holes (*Figure 11.a.I*). Fluoropolymer was not penetrated into microwells with interfacial control by ST structure [41, 42]. The topological liquid pinning phenomena cause the fluoropolymer solution hanging on the small holes. After complete drying of the solvent in an 85°C oven for 30 min, the deposited area with the fluoropolymer is turned into a hydrophobic surface (*Figure 11.a.II*). Time-lapse image shows the result in presence and absence of ST structure in solution-based surface modification processing (*Figure 11.b*). Dark circles at the liquid-air phase, visible only in the small hole area, show the impermeability of the fluoropolymer in heterogeneous through-hole. In contrast, homogenous through-hole platform allows the fluoropolymer solution to fill inside. After fluoropolymer coating, the device is treated with oxygen plasma at 50 W for 30 s, and then placed in an oven at 85°C for 15 min (*Figure 11.a.III*). It was confirmed that successfully modified to HIH surface by the measurement of contact angles. The contact angle of each materials in fabricated device was measured 99.4±3.2°, 21.6±1.1°, and 50.4±0.7°, respectively.

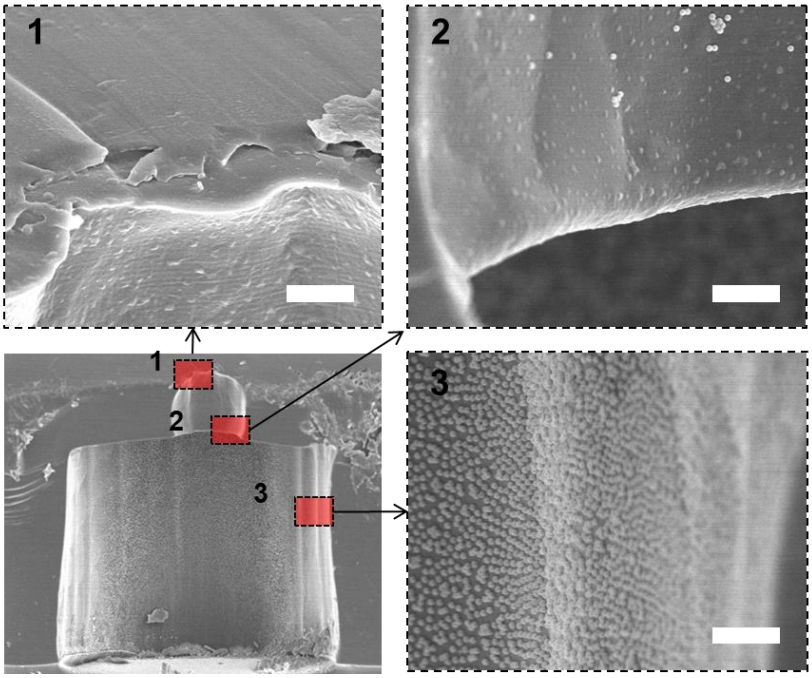

Figure 12. SAM image of HIH surface modified microwell cross-sectional side view. the microwell interior was treated with oxygen plasma and attached the amine group on the treated surface using aqueous 10% APTES and small hole side surface was deposited with 3M Novec 1720 fluoropolymer. The functionalization of APTES was determined by attachment of 200-nm carboxylated polystyrene nanoparticles. (Scale bar : 10 μm)

This method provides a unique advantage to end-users by enabling customized functionalization of hydrophilic surfaces. To demonstration, the microwell was treated with oxygen plasma and attached the amine group on the treated surface using aqueous 10% (3-aminopropyl) triethoxysilane (APTES) solution. Then, the device was baked at 85°C in an oven for 15 min. The confirmation of APTES functionality was proceeded with the suspension of negatively charged 200-nm carboxylated polystyrene particles (PS NPs) that was loaded into the microwell and then washed thoroughly with water. The fact that negatively charge 200-nm PS NPs in suspension state attach electrostatically only to the positively charged APTES-treated surfaces of the device was confirmed. As a result, only the interior of the microwell had lots of electrostatically attached particles (*Figure 12.3*) due to the positively charged amine group, whereas the exterior surfaces were clean and not functionalized with APTES (*Figure 12.1*). Partially attached particles in figure 12.2 suggest that the liquid-air interface of 3M Novec 1720 is formed in the vicinity of the inlet holes during the solution-processed fluoropolymer coating.

2.3.2 Self- partitioning with Hydrophilic-In-Hydrophobic Surface

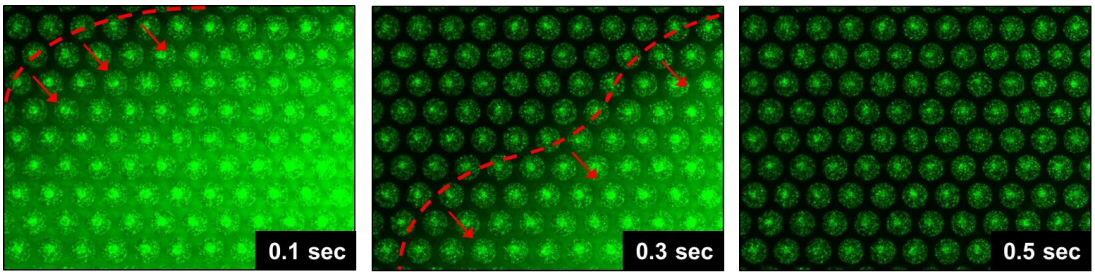

Figure 13. Self-partitioning with GFP microbial cells in LB. Red dash line represented liquid-air phase and self-partitioning occurred in 0.5 seconds.

Self-partitioning with HIH modified surface was conducted with GFP cells contain in LB (0.02% Amp, 0.001% F-127). To observe the process microscopically, cell suspension was dropped onto small hole-side surface and removed by a micropipette from the right side. As the time-sequenced in fluorescent images, cell suspension was pinched off uniformly at the small holes without leaving any residue or liquid on the hydrophobic surface (*Figure 13*). This homogeneous and promptly processible method was not dependent to user's proficient and might also be highly applicable in point-of-care applications like digital single-molecular detection [43]. Moreover, because the method can simply form a useful HIH surface without the necessity of costly and multi-step lithographic processes, it provides a wide range of functional groups that can be customized to make surfaces suitable for various biological surface affinities.

	Capacity Volume	Relative Throughput (in 3.8 cm x 5.5 cm)
Living Chip	50 nL	8,208 microwells
RT qPCR Nanowell Array	33 nL	6,485 microwells
NAPPA	5 nL	8,481 microwells
Fluid Array	1.3 nL	7,442 microwells
DS microwell Array	0.8 nL	150,000microwells

Table 2. Relative throughput with previous nL volume microwell array models [27,44-46]**.**

HIH surface modification increases the relative throughput of microwells in standard area. Table 2 shows the number of microwells that can be fabricated in the same area with previous well array devices with similar nL capacity volume. While the conventional models are in the range of 10^3 ~ 10^4 microwells, the DS microwell array deals with 10^5 scales with excellent partitioning. The improvement in partitioning and the minimization of the distance between neighboring microwells have breached the limits of throughput possible of microwell array devices.

2.4 Hatching-like Isolation with Double-Sided Microwell

2.4.1 Recent Target Cell Extraction Methods

	Extraction type	Support Materials	Resolution
SAPM (Self-Assembled particle Membrane) Bioreactor Array	UV polymerization and medium flow	PEGDA	~ 500 μm
PLACS (Pulse Laser triggered fluorescence activated cell sorter)	Pulse Laser trigger		~ 60 μm
Fluid Array	Capillary force		~ 360 μm
On Demand Release and Retrieval Microwell Array	UV photo-degradation	PEG hydrogel	20 μm
3 Dimension Droplet Array	Thermal detaching with infrared laser and medium flow	Low melting agarose	25 μm
DS (Double-Sided) Microwell Array	Physically punch hole	OSTEmer	0.31 μm

Table 3. Recent developed extraction methods for target cell isolation. Optical instruments-based extraction is more precise than handling. However, these optics can have adverse effects on cells, and it reduce applicable cell range. The DS microwell array was more cell-friendly extraction because it is a purely physical approach and it has similar high resolution with 0.31 μm [27, 35-36, 47-48].

Target cell isolation with microfluidics has been attracted due to high selectivity and purity. For example, J.W Lim et al. extracted target superior strain from 10^6 different libraries using different mass fluid and capillary force [27]. Through this fluid array, specific strains with high free fatty acid (FFAs) production were selected and related mutant genes were identified [49]. Optical instruments-based extraction such as laser or UV were also developed for convenient and better precision than liquid handlings [35-36, 47-48]. André J. van der Vlies et al. trapped the microbial cells with poly ethylene glycol (PEG) hydrogels and extracted a target microwell using the characteristics of photo-degradability materials with UV [35]. On the other hand, Sébastien Sart et al. burn off the agarose attached to the wall of microwell using infrared laser and extracted with additional medium flow [36]. Both were noteworthy due to high-precision and suitable to automation systems. However, cell death by laser-generated intense heat and genetic mutation by UV lead to the reduction of applicable cell range.

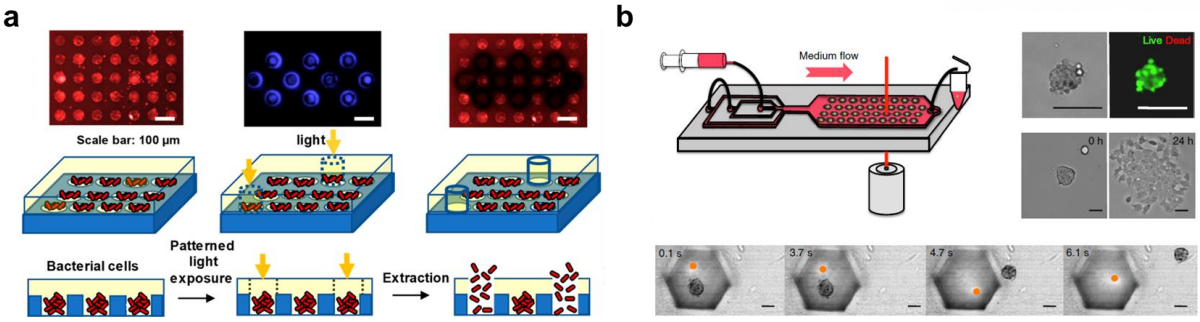

Figure 14. Recent target cell extraction methods using optical instruments. (a) The specific region of photo-degradable hydrogel (PEG hydrogel) was dissolved by UV [35]. (b) The cured agarose droplet in microwells was detached with the strong heat generation by infrared laser and extracted with an additional medium flow [36].

2.4.2 Automatic Extraction System for High-throughput Screening Optimization

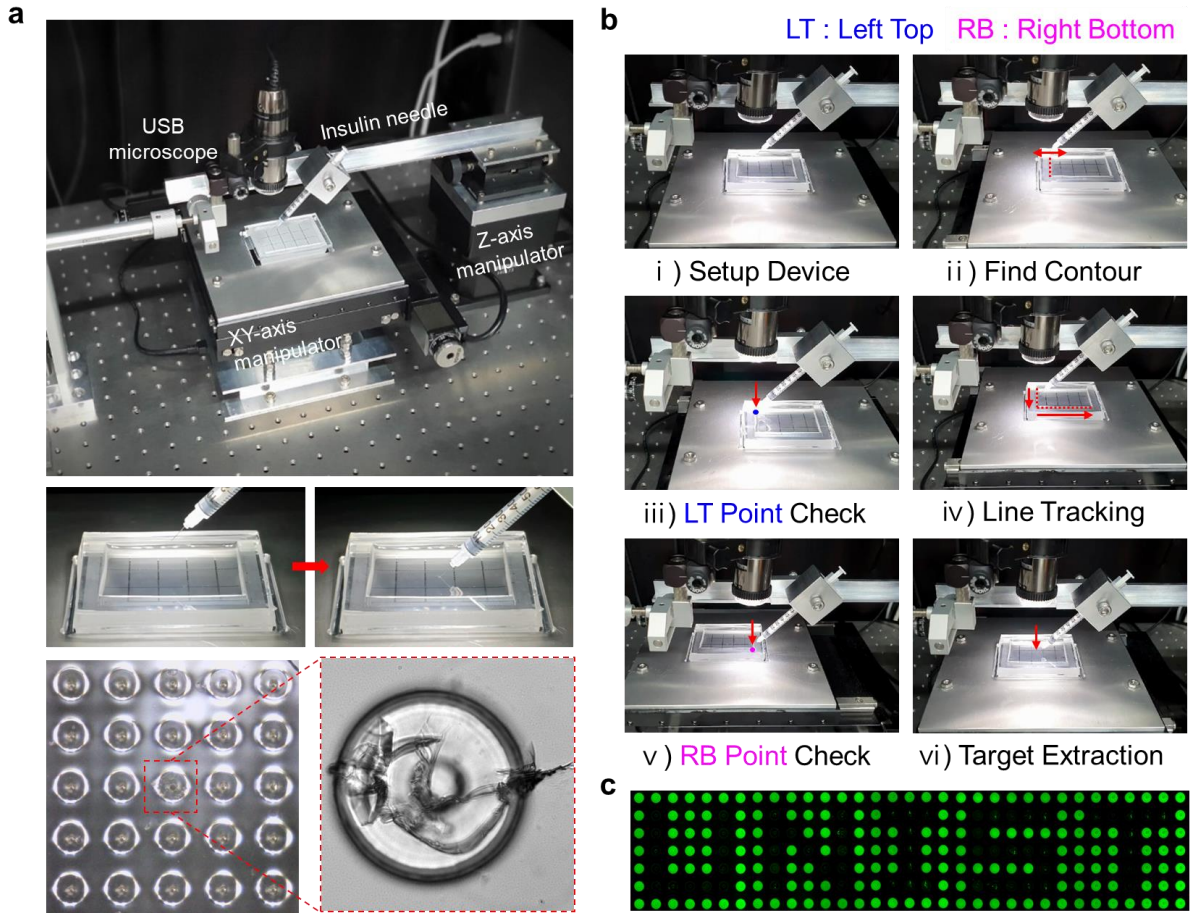

Figure 15. Automatic cell extractor for target isolation in high-throughput screening. (a) Real image of customized cell extractor. The bottom shows the punched H-PDMS layer and crack-based vertical channel forming process. (b) It describes the order of automated extraction process controlled by LabVIEW-based software. (c) Demonstration of cell extractor for high-precision using FITC solution. (PBS 1X, 0.01% F-127)

This research optimizes the processing time not only high-throughput microwell array platform with

HIH partitioning, but also automated extraction system. The automation minimized the selective extraction within 5 seconds and scanning target coordinate was more precise through software calibration. It was progressed with a hand-made cell extractor which is customized to the DS microwell array. Cell extractor was consisted with USB-microscope, XY-axis motorized stage for positioning microwells to the extraction site, and Z-axis manipulator for leveling a commercial insulin needle (*Figure 15.a*). This installation was operated by bespoke software that was revised from distribution SDK (*Figure 15.b*). It finds the coordinates of the target microwell by a few steps. Through USB microscope live video, all of real-time data was transported. First, it detects the left contour line of microwell array. Second, it goes straight up the line tracking and find the top left point (TL) and Right bottom (RB) point. The z value of the LT point and RB point, measured with an insulin needle, is used to calculate the slope of the chip and to estimate the z value of the target microwell. Lastly, based on the values obtained, the coordinates of the target microwell are calculated and punched by lowering the insulin needle with the z-manipulator. Figure 15.c shows the high-precision of automatic extraction device using FITC solution (50 μM FITC, 1X PBS, 0.01% F-127). The microwells in which the vertical microchannel were formed by the insulin needles lost the fluorescent light by diffusion, and the extraction was performed in the form of UNIST letters.

2.4. Characterization of Hatching-like Isolation

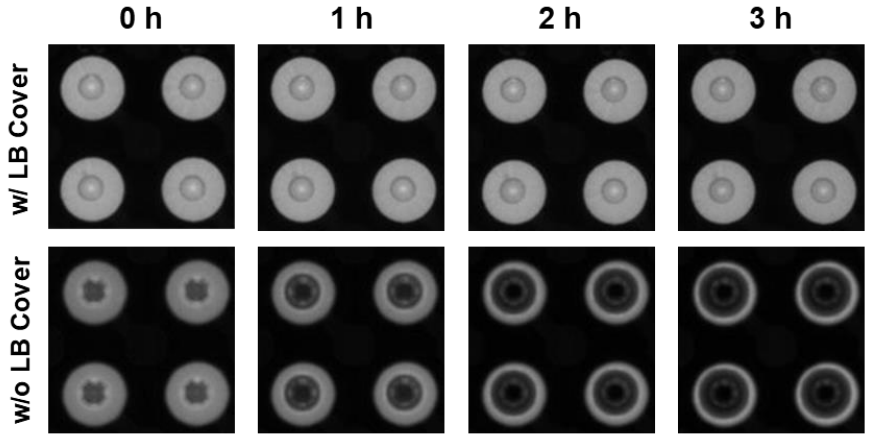

Figure 16. Partitioned FITC solution with LB cover. 3 hours later, the absence of LB cover shows dark gray circle that evaporated site compared with presence of LB cover.

Before setup the extraction, H-PDMS was transferred to culture membrane and sealing the small holes with PDMS slab. In series, microwells covered with H-PDMS was guarded from rapid dehydration with LB medium (*Figure 16*). The clean wall PDMS confine the medium as a container and could be coupled to the extraction process. Water vapor in the microwells can escape into the porous structure of the

PDMS, but the LB medium prevents it. Thus, no matter how long the extraction proceeds, the micro sample does not evaporate.

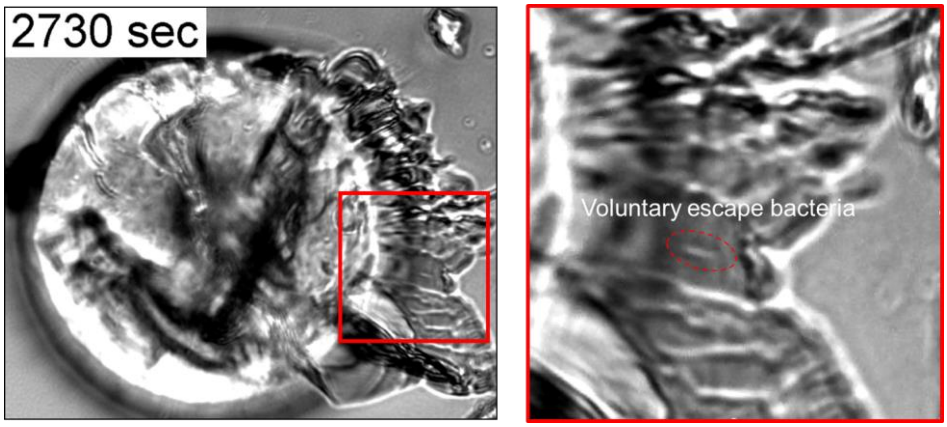

Figure 17. Hatching-like isolation process with voluntary extracted cells. The image of spontaneous escaped bacteria in the vertical microchannels was taken in 2730 sec at 30X magnification.

LB medium cover also provides incubation space that directly connected with the punched target microwell via crack-based vertical microchannel. The vertical microchannel was formed on brittle H-PDMS by the insulin needle and it resembles the hatching egg surface appearance. Target microbes were voluntary extracted with random walk motility through vertical microchannel and it was captured in bright field images at 30X magnification (*Figure 17*).

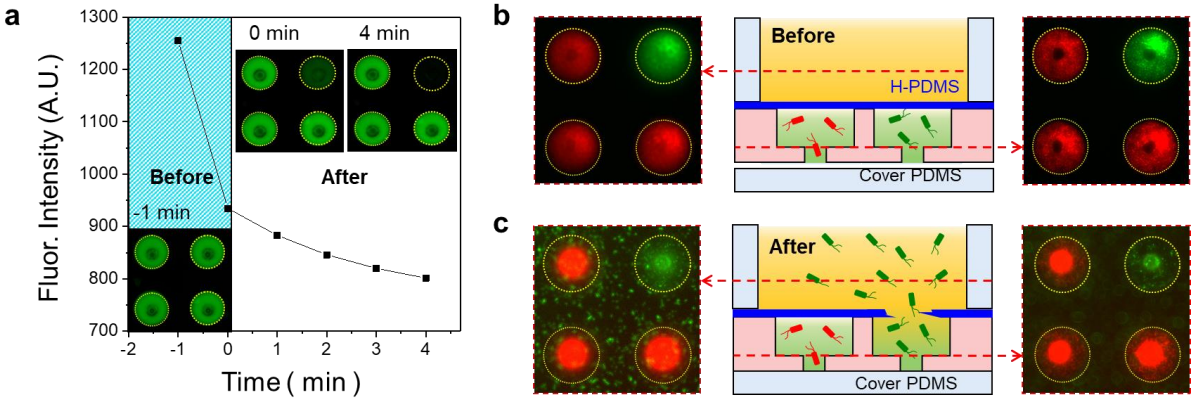

Figure 18. Characterization of hatching-like isolation. (a) The FITC solution (PBS 1X, 0.01% F-127) mass transfer rate with diffusion was described with the fluorescence intensity graph. Sky blue box indicates handling time period after punching process. (b, c) GFP and RFP fluorescence images of different focal points for selective extraction confirmation. Each of them indicates before extraction state and the result of forming vertical microchannels with incubated 6 hours.

The hatching-like isolation, which named from cleaved H-PDMS and the escaped bacteria from it, was characterized in terms of the mass transfer completion time and extraction selectivity. Diffusion rate

was measure with fluorescence intensity of FITC solution (*Figure 18.a*). Sky blue box indicated the time taken to move to the microscope after extraction. The fluorescence intensity dropped sharply after extraction and completely disappeared after 4 minutes to equal background noise. The graph indicates that the advection-dominant mass transfer of FITC at the moment of inserting the needles is followed by the diffusion of FITC. For testing extraction selectivity, two phenotypically different bacterial cells were partitioning in microwell array (*Figure 18.b*). Cell suspension (GFP cells : RFP cells = 1 : 50) was loaded, and then finding occasional single-GFP-cell microwell with nearby three single-RFP-cell microwells for better visualization. The microwells containing target cells (GFP) was punched and conducted hatching-like isolation. After culturing 6 hours, fluorescence imaging was performed focusing on small holes and media layer. When sealing to the culture membrane with cover PDMS (= PDMS slab), air pockets are formed in small holes. Although the distribution of cells was observed in the form of donuts early on, it appears that cells deposit in small hole spaces filled over time to express strong fluorescence signals. GFP and RFP cells were well expressed and grown in each microwell at the small hole focal point, whereas only GFP cells was distributed in the media layer. As a result, selective extraction was confirmed that the 100% composition of GFP cells in the media layer and H-PDMS well-traps undesirable RFP cells in other microwells.

III. Application of Stepped Through-hole Structure and Double-Sided Microwell

3.1 Chemical Dosing with Humidity Control System

In bio-medical studies, lots of chemical candidates, which has high potential to be vaccine or therapeutic remedy, were prescreened with high-throughput bio-assay. However, pharmaceutical assistants require exorbitant cost, intensive labor and large-scale throughput platform with same condition. For this reason, numerous chemical manipulation techniques were developed such as barcoded-beads, lysis buffer droplet, or genetic inducers [50]. For example, Su Eun Chung et al. developed hydrogel based chemical-laden microparticles for high-throughput multiplexed bioassays [30]. Hydrogel microparticles absorbed anti-cancer drug and partitioned by partipetting skills into microarrays containing osteosarcoma cells. The absorbed anti-cancer drug was released and transferred to osteosarcoma cells with diffusion.

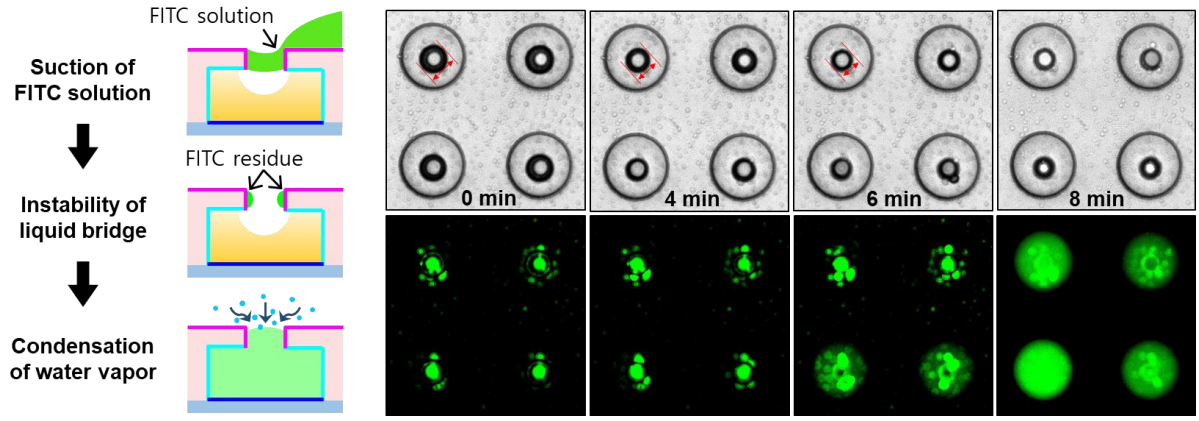

Figure 20. Schematic chemical dosing and time-lapse image of vapor supply by condensation. Red arrows in the bright-field image highlight the diameter of the liquid-air interface formed in the microwell, showing a decrease in the diameter during condensation.

Chemical dosing with stepped through-hole structure are also expected to have great significance in a similar context. This method uses selective condensation based on the ST structure and HIH surface to inject the same chemical into cells in each microwell simultaneously without cross contamination (*Figure 20*). In order to visualize the chemical dosing, experiments were conducted with FITC fluorescent materials (250 μM FITC, 1X PBS, 0.002% F-127), and the used device was already subjected to HIH surface treatment. The approach was similar with solution-processed fluoropolymer coating. After we dropped FITC solution on the top side of the device containing the LB medium, we

removed the bulk solution by suction through a micropipette. FITC fluorescence signal was tracked at around small holes. The red arrows in the bright-field image show air-liquid phase and simultaneous fluorescence imaging confirmed that it was separated from the FITC residue. The microwell, which segregated the reagent and FITC residues, showed a fluorescence signal only in the small hole region, but the result is different due to changes in temperature and humidity from 38°C and RH = 95% to 30°C and RH = 99%. Interestingly, the water vapor in the air does not condense on the small hole side surface and concretized inside the microwell interior. Such large difference in the flux of vapor condensation may be attributed to the differences in wettability between the liquid and hydrophobic surface [51]. As the fluorescence image in elapsed 6 minutes, the whole inside of the below two microwells suddenly expressed weak FITC fluorescence signals, and it was confirmed that the middle part of the microwell has a small black circle that is different with previous one. The liquid pinning was an unstable state in small holes so that the circle shape of FITC residues transformed into a donut shape. The vapor raises the surface of the reagent inside the microwell through those black holes and allows it to react with FITC residues. As a result, medium contacted and dissolved the FITC residues without any cross-contamination with nearby microwells.

3.2 Buffer Exchange with Stepped Through-hole Structure

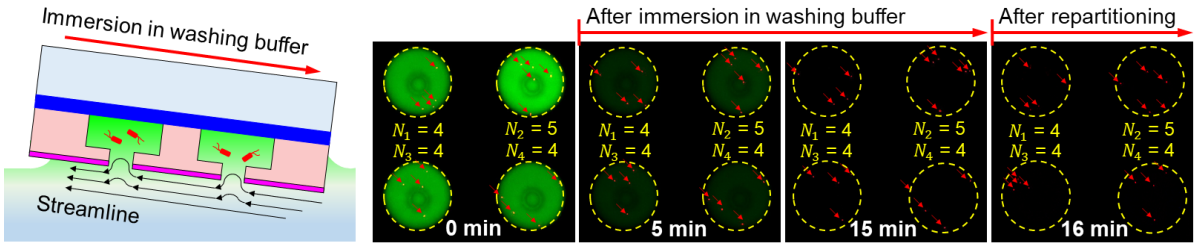

Figure 19. Schematic illustrations and fluorescence images of buffer exchange. The device was immersed in clean water and washed out FITC (PBS 1X, 0.01% F-127) from the microwells. Red arrows in time-lapse images highlight the RFP cells to show the constant number even after repartitioning.

Buffer washing technique in bio-assays is necessary to long-term culture process or serial multi-drug screening. DS Microwell array is common dead-end microfluidic platforms is limited mass transfer by the bottleneck structure. However, as the illustration of a cross-sectional side view and time-lapse fluorescence images, the batch type of microwell array with ST structure shows buffer exchange is possible without microchannel insertion (*Figure 19*). To demonstrate, the device containing RFP cells in a solution (50 μM FITC, 1X PBS, 0.001% F-127) was immersed and floated in fresh water. When the device was lifted, courtesy of the stepped through-hole structure, the advection flow only affected the small hole entrance, allowing the constant number of RFP cells in each microchamber even after

repartitioning. On the other hand, FITC fluorescence intensity was faded out in 15 minutes. This result was caused by diffusion-based mass transfer and it means the inside of the microwell was replaced with a clean buffer. However, it appears to be suitable for single-cell applications because high-density cells have high potentials to be leak. This washing method can be further developed with an additional microfluidic layer that can guide the continuous flow of fresh medium or washing buffer.

3.3 High-throughput Screening Demonstration: Rare Cell Isolation

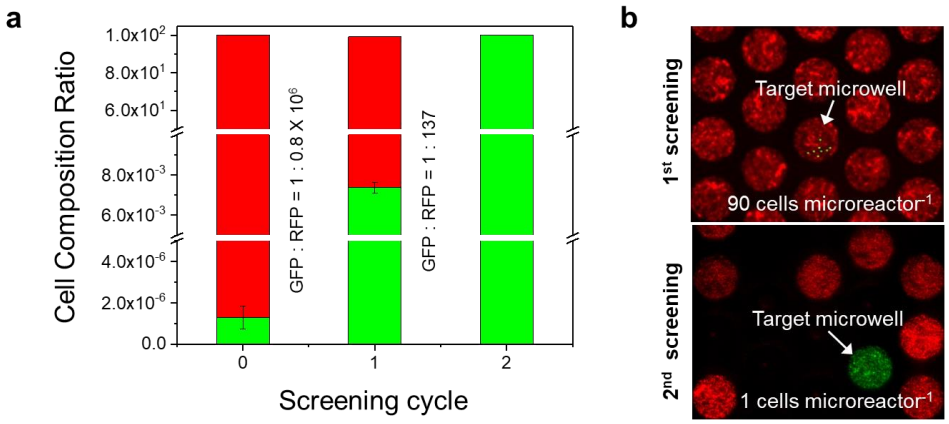

Figure 21. High-throughput screening demonstration with rare cell isolation. (a) The cell composition ratio of extracted samples with hatching-like isolation method. There were two screening cycles in total, and the GFP cell composition ratio increasing from 0.00013% to 0.73% and 100%, respectively. (b) fluorescence image in each screening culture. The 1st screening was diluted with an average of 90 cells per chamber to increase throughput, whereas 2nd screening was performed with dilution to single cell level to increase the precision of cell selectivity.

For high-throughput screening demonstration of DS microwell array, the rare cell isolation test proceeded with a proof-of-concept experiment. Two kinds of genetic-modified cells with different phenotypes were used, mixed at a ratio of 1 to 10^6, and the target GFP cell was selected from undesired RFP cells (*Figure 21*). And then, the cell composition ratio of extracted sample with hatching-like isolation method was confirmed with 10 μm height microchannel. There are two screening cycles in total, and the loading cell density (cells/microwell) is different in each screening cycle. The density of cells loaded is important because the number of cells in one microwell times the number of microwells in a device determines the identifiable throughput of one chip. Therefore, initial loading cell density in 1st screening was calculated considering total throughput and 2nd screening was conducted with a single-cell level for high-selectivity.

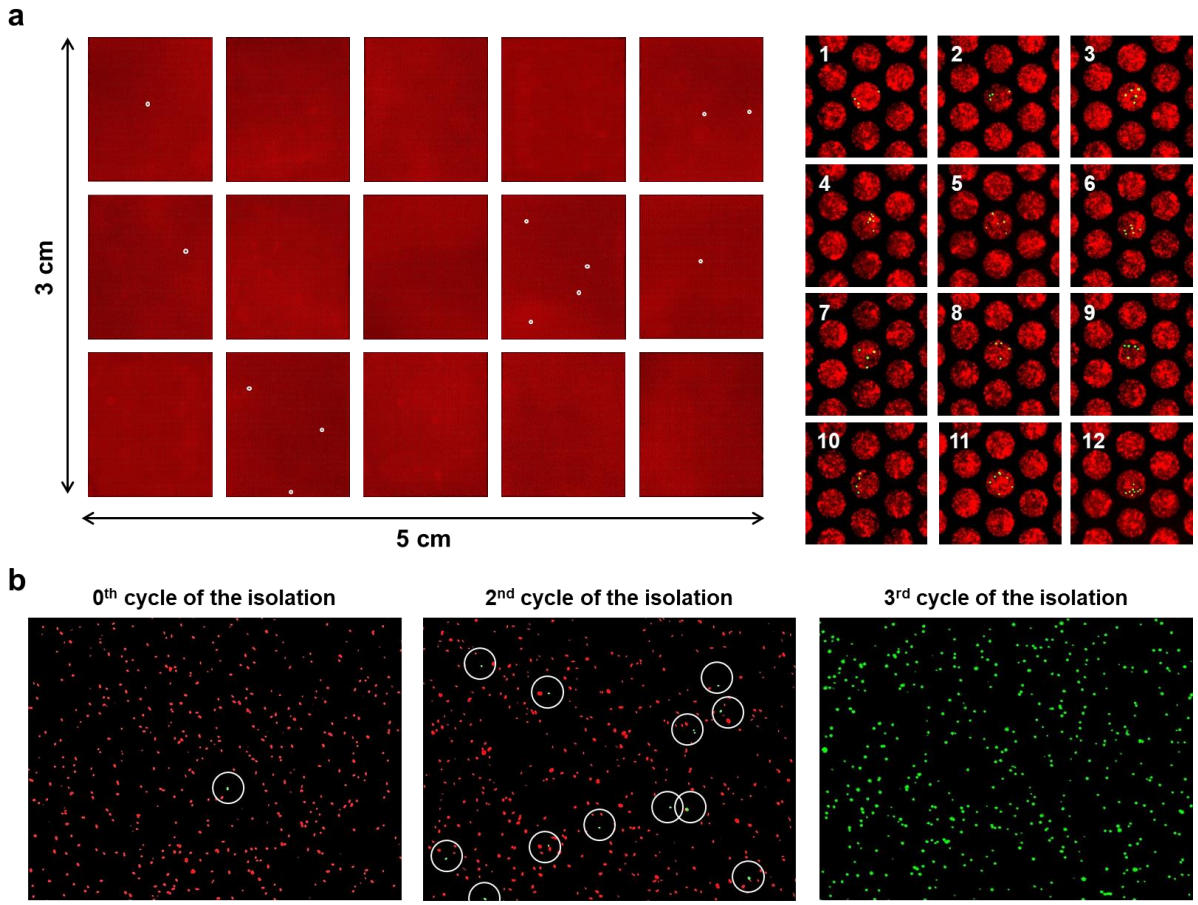

Figure 22. 1st screening large area scanning result and cell composition image. (a) The image was taken at 10X magnification, and each photographic piece were combined with image stitching technique. Consequently, 12 coordinates of target microwell were detected in 1st screening scan data. (b) Fluorescence image of cell composition in each screening cycle with 10 μm height microchannels.

Mixture cell suspension in microwell array was cultured for 10 hours to reach the stationary phase and scanned all microwells with Scanslide software function that automatically scanning the large-scale area (*Figure 22*). The scanning time was very short because the number of wells captured on one screen is much higher proportional to the throughput. After scanning at 4X magnification, the detected fluorescence signal of target cells can be scanned within 5 minutes and the detailed coordinates are identified at 10X magnification. Since the total throughput is 10^7 (number of microwells×number of loading cells in one microwell = $1.5 \times 10^5 \times 90$), theoretically, the 1st screening should yield 13 microwells that containing GFP cells. Consequently, 12 coordinates were detected, and the rare cell composition ratio of extracted sample was 0.73% as shown in figure 22.a. The ratio of GFP cells and RFP cells in one microwell is 1: 90, the statistic numerical rate is 1.1%. The experimental values of GFP cell composition were similar to the statistical results, indicating that follows the numerical theory. 2nd screening was progressed with a similar manner of the 1st screening cycle except single-cell level

loading density. Each microwell was distributed from 0 to 6 according to the Poisson distribution, which was intended to obtain an extracted sample consisting only of GFP cells. As a result, GFP cell was successfully isolated from a million to one ratio mixture cell suspension in 2 screening cycle. This proof experiments are only intended to show the potential of high throughput screening, which can deal with 10^8 to 10^9 samples using multiple devices in parallel. Although many technologies are still being developed for the partitioning, chemical dosing, a cell extraction in high-throughput studies, there is a lack of research on integrated systems that encompass all technologies. It does not show a specialized study for one biological finding, but efforts to integrate of each part including partitioning, dosing, screening, and extraction, to cover various kinds of biological assays.

IV. Conclusion

In this dissertation, a novel microfluidic bioreactor was developed to increase throughput for advanced microbial sample handlings. As described in the introduction, the throughput has a trade-off with partitioning ability in the usual microwell platform. However, this microwell array shows not only increased throughput with ST and DS structure, but also multi-functions that includes self-partitioning, buffer exchange, chemical dosing, and selective extraction for high-throughput bio-application. DS microwell array was integrated with a heterogeneous through-hole membrane with different hole sizes. The small hole was easily open accessible and each microwell was fabricated into hydrophobic-in-hydrophilic. The microwell array has 150,000 separated micro-environments and it was self-compartmentalized by HIH surface. And then, it was confirmed that cell growth density in microwell array is 2.2×10^9 cells/mL that has similar culture environment with shaking incubator (= 2.3×10^9 cells/mL). The ST structure is involved in surface modification or chemical dosing, while the DS structure is used in selective cell extraction. It was conducted physically with an insulin needle by cracking the brittle H-PDMS that covered large holes-side of microwells. The vertical microchannels on the punched microwell provides the connection with LB medium and allows spontaneous extraction of target microbes. As a result, stationary state of microbial cells escaped from saturated microwell to fresh medium. Lastly, I demonstrate practical bio-application for high-throughput screening with rare cell isolation test. The initial cell population ratio is $1{:}10^6$ and it was screened with customized automatic screening system. In two screening cycle, 100% pristine sample that composed with only rare cells was isolated from undesired cluster. Although this study did not carry out real microbial studies for biological discovery, it is believed that it contributed greatly by introducing various high-throughput bio-application.

Reference

1. Shim, J.-u.; Olguin, L. F.; Whyte, G.; Scott, D.; Babtie, A.; Abell, C.; Huck, W. T. S.; Hollfelder, F., Simultaneous Determination of Gene Expression and Enzymatic Activity in Individual Bacterial Cells in Microdroplet Compartments. *Journal of the American Chemical Society* **2009**, *131* (42), 15251-15256.

2. Tong, A. H. Y.; Evangelista, M.; Parsons, A. B.; Xu, H.; Bader, G. D.; Pagé, N.; Robinson, M.; Raghibizadeh, S.; Hogue, C. W. V.; Bussey, H.; Andrews, B.; Tyers, M.; Boone, C., Systematic Genetic Analysis with Ordered Arrays of Yeast Deletion Mutants. **2001**, *294* (5550), 2364-2368.

3. Lee, J.; Kim, M.; Park, J.; Kim, T., Self-assembled particle membranes for in situ concentration and chemostat-like cultivation of microorganisms on a chip. *Lab Chip* **2016**, *16* (6), 1072-80.

4. Yeh, E.-C.; Fu, C.-C.; Hu, L.; Thakur, R.; Feng, J.; Lee, L. P., Self-powered integrated microfluidic point-of-care low-cost enabling (SIMPLE) chip. **2017**, *3* (3), e1501645.

5. James, T.; Mannoor, M. S.; Ivanov, D. V., BioMEMS -Advancing the Frontiers of Medicine. *Sensors (Basel)* **2008**, *8* (9), 6077-6107.

6. Kaminski, T. S.; Garstecki, P., Controlled droplet microfluidic systems for multistep chemical and biological assays. *Chem Soc Rev* **2017**, *46* (20), 6210-6226.

7. Kim, S. C.; Clark, I. C.; Shahi, P.; Abate, A. R., Single-Cell RT-PCR in Microfluidic Droplets with Integrated Chemical Lysis. *Anal Chem* **2018**, *90* (2), 1273-1279.

8. Prakash, R.; Pabbaraju, K.; Wong, S.; Wong, A.; Tellier, R.; Kaler, K., Multiplex, Quantitative, Reverse Transcription PCR Detection of Influenza Viruses Using Droplet Microfluidic Technology. *Micromachines* **2014**, *6* (1), 63-79.

9. Fang, X.; Chen, H.; Yu, S.; Jiang, X.; Kong, J., Predicting viruses accurately by a multiplex microfluidic loop-mediated isothermal amplification chip. *Anal Chem* **2011**, *83* (3), 690-5.

10. Kim, M.; Lim, J. W.; Kim, H. J.; Lee, S. K.; Lee, S. J.; Kim, T., Chemostat-like microfluidic platform for highly sensitive detection of heavy metal ions using microbial biosensors. *Biosens Bioelectron* **2015**, *65*, 257-64.

11. Liu, Y.; Li, G., A power-free, parallel loading microfluidic reactor array for biochemical screening. *Sci Rep* **2018**, *8* (1), 13664.

12. Yang, G.; Withers, S. G., Ultrahigh-throughput FACS-based screening for directed enzyme evolution. *Chembiochem* **2009**, *10* (17), 2704-15.

13. Becker, S.; Schmoldt, H. U.; Adams, T. M.; Wilhelm, S.; Kolmar, H., Ultra-high-throughput screening based on cell-surface display and fluorescence-activated cell sorting for the identification of novel biocatalysts. *Curr Opin Biotechnol* **2004**, *15* (4), 323-9.

14. Kang, D. K.; Ali, M. M.; Zhang, K.; Huang, S. S.; Peterson, E.; Digman, M. A.; Gratton, E.; Zhao, W., Rapid detection of single bacteria in unprocessed blood using Integrated Comprehensive Droplet Digital Detection. *Nat Commun* **2014**, *5*, 5427.

15. Golberg, A.; Yarmush, M. L.; Konry, T., Picoliter droplet microfluidic immunosorbent platform for point-of-care diagnostics of tetanus. *Microchimica Acta* **2013**, *180* (9-10), 855-860.

16. Liu, L.; Dalal, C. K.; Heineike, B. M.; Abate, A. R., High throughput gene expression profiling of yeast colonies with microgel-culture Drop-seq. *Lab Chip* **2019**, *19* (10), 1838-1849.

17. Kumar, P. T.; Vriens, K.; Cornaglia, M.; Gijs, M.; Kokalj, T.; Thevissen, K.; Geeraerd, A.; Cammue, B. P.; Puers, R.; Lammertyn, J., Digital microfluidics for time-resolved cytotoxicity studies on single non-adherent yeast cells. *Lab Chip* **2015**, *15* (8), 1852-60.

18. Vajrala, V. S.; Sekli Belaidi, F.; Lemercier, G.; Zigah, D.; Rigoulet, M.; Devin, A.; Sojic, N.; Temple-Boyer, P.; Launay, J.; Arbault, S., Microwell array integrating nanoelectrodes for coupled opto-electrochemical monitorings of single mitochondria. *Biosens Bioelectron* **2019**, *126*, 672-678.

19. Binder, D.; Drepper, T.; Jaeger, K. E.; Delvigne, F.; Wiechert, W.; Kohlheyer, D.; Grunberger, A., Homogenizing bacterial cell factories: Analysis and engineering of phenotypic heterogeneity. *Metab Eng* **2017**, *42*, 145-156.

20. Brouzes, E.; Medkova, M.; Savenelli, N.; Marran, D.; Twardowski, M.; Hutchison, J. B.; Rothberg, J. M.; Link, D. R.; Perrimon, N.; Samuels, M. L., Droplet microfluidic technology for single-cell high-throughput screening. **2009**, *106* (34), 14195-14200.

21. Kim, H. S.; Devarenne, T. P.; Han, A., A high-throughput microfluidic single-cell screening platform capable of selective cell extraction. *Lab Chip* **2015**, *15* (11), 2467-75.

22. Curtis, T. P.; Sloan, W. T.; Scannell, J. W., Estimating prokaryotic diversity and its limits. **2002**, *99* (16), 10494-10499.

23. Schloss, P. D.; Handelsman, J., Status of the microbial census. *Microbiol Mol Biol Rev* **2004**, *68* (4), 686-91.

24. Colin, P. Y.; Kintses, B.; Gielen, F.; Miton, C. M.; Fischer, G.; Mohamed, M. F.; Hyvonen, M.; Morgavi, D. P.; Janssen, D. B.; Hollfelder, F., Ultrahigh-throughput discovery of promiscuous enzymes by picodroplet functional metagenomics. *Nat Commun* **2015**, *6*, 10008.

25. Yu, F. B.; Blainey, P. C.; Schulz, F.; Woyke, T.; Horowitz, M. A.; Quake, S. R., Microfluidic-based mini-metagenomics enables discovery of novel microbial lineages from complex environmental samples. *Elife* **2017**, *6*.

26. Sjostrom, S. L.; Bai, Y.; Huang, M.; Liu, Z.; Nielsen, J.; Joensson, H. N.; Andersson Svahn, H., High-throughput screening for industrial enzyme production hosts by droplet microfluidics. *Lab Chip* **2014**, *14* (4), 806-13.

27. Lim, J. W.; Shin, K. S.; Moon, J.; Lee, S. K.; Kim, T., A Microfluidic Platform for High-Throughput Screening of Small Mutant Libraries. *Anal Chem* **2016**, *88* (10), 5234-42.

28. Szita, N.; Polizzi, K.; Jaccard, N.; Baganz, F., Microfluidic approaches for systems and synthetic biology. *Curr Opin Biotechnol* **2010**, *21* (4), 517-23.

29. Wang, Y.; Southard, K. M.; Zeng, Y., Digital PCR using micropatterned superporous absorbent array chips. *Analyst* **2016**, *141* (12), 3821-31.

30. Eun Chung, S.; Kim, J.; Yoon Oh, D.; Song, Y.; Hoon Lee, S.; Min, S.; Kwon, S., One-step pipetting and assembly of encoded chemical-laden microparticles for high-throughput multiplexed bioassays. *Nat Commun* **2014**, *5*, 3468.

31. Gowa Oyama, T.; Barba, B. J. D.; Hosaka, Y.; Taguchi, M., Single-step fabrication of polydimethylsiloxane microwell arrays with long-lasting hydrophilic inner surfaces. *Applied Physics Letters* **2018**, *112* (21).

32. Zandi Shafagh, R.; Decrop, D.; Ven, K.; Vanderbeke, A.; Hanusa, R.; Breukers, J.; Pardon, G.; Haraldsson, T.; Lammertyn, J.; van der Wijngaart, W., Reaction injection molding of hydrophilic-in-hydrophobic femtolitre-well arrays. *Microsyst Nanoeng* **2019**, *5*, 25.

33. Lee, D. W.; Choi, Y. S.; Seo, Y. J.; Lee, M. Y.; Jeon, S. Y.; Ku, B.; Kim, S.; Yi, S. H.; Nam, D. H., High-throughput screening (HTS) of anticancer drug efficacy on a micropillar/microwell chip platform. *Anal Chem* **2014**, *86* (1), 535-42.

34. Gole, J.; Gore, A.; Richards, A.; Chiu, Y. J.; Fung, H. L.; Bushman, D.; Chiang, H. I.; Chun, J.; Lo, Y. H.; Zhang, K., Massively parallel polymerase cloning and genome sequencing of single cells using nanoliter microwells. *Nat Biotechnol* **2013**, *31* (12), 1126-32.

35. Van der Vlies, A. J.; Barua, N.; Nieves-Otero, P. A.; Platt, T. G.; Hansen, R. R., On Demand Release and Retrieval of Bacteria from Microwell Arrays Using Photodegradable Hydrogel Membranes. *ACS Applied Bio Materials* **2018**, *2* (1), 266-276.

36. Sart, S.; Tomasi, R. F.; Amselem, G.; Baroud, C. N., Multiscale cytometry and regulation of 3D cell cultures on a chip. *Nat Commun* **2017**, *8* (1), 469.

37. Hsieh, K.; Zec, H. C.; Chen, L.; Kaushik, A. M.; Mach, K. E.; Liao, J. C.; Wang, T. H., Simple and Precise Counting of Viable Bacteria by Resazurin-Amplified Picoarray Detection. *Anal Chem* **2018**, *90* (15), 9449-9456.

38. Armani, D.; Liu, C.; Aluru, N. In Re-configurable fluid circuits by PDMS elastomer micromachining, Technical Digest. *IEEE* **1999**; pp 222-227.

39. Zhu, Q.; Xu, Y.; Qiu, L.; Ma, C.; Yu, B.; Song, Q.; Jin, W.; Jin, Q.; Liu, J.; Mu, Y., A scalable self-priming fractal branching microchannel net chip for digital PCR. *Lab Chip* **2017**, *17* (9), 1655-1665.

40. Liu, T. L.; Kim, C.-J. C., Turning a surface superrepellent even to completely wetting liquids. **2014**, *346* (6213), 1096-1100.

41. Zhou, Q.; Lee, K.; Kim, K. N.; Park, J. G.; Pan, J.; Bae, J.; Baik, J. M.; Kim, T., High humidity- and contamination-resistant triboelectric nanogenerator with superhydrophobic interface. *Nano Energy* **2019**, *57*, 903-910.

42. Li, J.; Zhou, X.; Li, J.; Che, L.; Yao, J.; McHale, G.; Chaudhury, M. K.; Wang, Z., Topological liquid diode. **2017**, *3* (10), eaao3530.

43. Rissin, D. M.; Kan, C. W.; Campbell, T. G.; Howes, S. C.; Fournier, D. R.; Song, L.; Piech, T.; Patel, P. P.; Chang, L.; Rivnak, A. J.; Ferrell, E. P.; Randall, J. D.; Provuncher, G. K.; Walt, D. R.; Duffy, D. C., Single-molecule enzyme-linked immunosorbent assay detects serum proteins at subfemtomolar concentrations. *Nat Biotechnol* **2010**, *28* (6), 595-9.

44. Brenan, C.; Morrison, T.; Stone, K.; Heitner, T.; Katz, A.; Kanigan, T.; Hess, R.; Kwon, S.-J.; Jung, H.-C.; Pan, J.-G., Massively parallel microfluidics platform for storage and ultra-high-throughput screening. *SPIE:* **2002**; Vol. 4626.

45. Ocampo, A.; Barrientos, A., From the bakery to the brain business: developing inducible yeast models of human neurodegenerative disorders. *BioTechniques* **2008**, *45* (4S), vii-xiv.

46. Takulapalli, B. R.; Qiu, J.; Magee, D. M.; Kahn, P.; Brunner, A.; Barker, K.; Means, S.; Miersch, S.; Bian, X.; Mendoza, A.; Festa, F.; Syal, K.; Park, J. G.; LaBaer, J.; Wiktor, P., High density diffusion-free nanowell arrays. *J Proteome Res* **2012**, *11* (8), 4382-91.

47. Wu, T. H.; Chen, Y.; Park, S. Y.; Hong, J.; Teslaa, T.; Zhong, J. F.; Di Carlo, D.; Teitell, M. A.; Chiou, P. Y., Pulsed laser triggered high speed microfluidic fluorescence activated cell sorter. *Lab Chip* **2012**, *12* (7), 1378-83.

48. Lee, J.; Park, J.; Kim, T., Dynamic Culture and Selective Extraction of Target Microbial Cells in Self-Assembled Particle Membrane-Integrated Microfluidic Bioreactor Array. *Anal Chem* **2019**, *91* (9), 6162-6171.

49. Lim, J. W.; Shin, K. S.; Ryu, Y. S.; Lee, Y.; Lee, S. K.; Kim, T., High-Throughput Screening of Acyl-CoA Thioesterase I Mutants Using a Fluid Array Platform. *ACS Omega* **2019**, *4* (26), 21848-21854.

50. Fan, H. C.; Fu, G. K.; Fodor, S. P., Expression profiling. Combinatorial labeling of single cells for gene expression cytometry. *Science* **2015**, *347* (6222), 1258367.

51. Boreyko, J. B.; Hansen, R. R.; Murphy, K. R.; Nath, S.; Retterer, S. T.; Collier, C. P., Controlling condensation and frost growth with chemical micropatterns. *Sci Rep* **2016**, *6*, 19131.

Acknowledgment

First, I would like to appreciate my advisor Professor Taesung Kim. It is not possible a great insight in research without his supports and advices. He held individual meeting every Tuesday and gave directions for the study as it progressed. He also guided me research life by giving examples of appropriate analogies and personal experiences. Not only Professor Taesung Kim, also other thesis committee members were good mentors. Professor Sung Kuk Lee gave advice on practical microbial application, and Professor Tae-eun Park helped to follow-up study with abundant knowledge of animal cell culture.

And thanks to my lab members Dogyeong Ha, Ji-won Lim, Jongwan Lee, Jun Gyu Park, Kyunghun Lee, Qitao Zhou, Sangjin Seo, Wooyeong Lim, Youngchul Chae, Yeonghoon Jeong and especially Juyeol Bae. From the internship to early graduate school, Dr. Ji-won Lim guided me with microbial research under the theme of oxygen gradient for aerotaxis. Throughout my laboratory life, I have been learned lots of techniques and knowhow such as photo-lithography, soft-lithography, microbial handlings etc. Those courses were necessary as a researcher, and I'm proud of my own development. Juyeol Bae designed and wrote "High -throughput Microbial Assays using Double-Sided Microwells with a Stepped Through-Hole Membrane" with me. In this process, he trained me all aspects of research in experimental design know-how, paper writing, and technical handlings. He is a senior graduate student and has shown a lot of respect.

Lastly, I would like to give this glory to my parents. My father, Jaesung Ju, is a role model who has demonstrated his patience and passion of research through 40 years of butterfly studies. My mother, Jin Ok Heo, always devoted love for me. With her care and spiritual support, I was able to live a psychologically comfortable graduate life.

And I want to finish it with this comment.

"Be patient, succeed and win"